



## PAPER

[View Article Online](#)  
[View Journal](#) | [View Issue](#)Cite this: *Mater. Adv.*, 2023,  
4, 3351

# Facile synthesis of 2-aza-9,10-diphenylanthracene and the effect of precise nitrogen atom incorporation on OLED emitters performance†

Evan R. Darzi, Dane A. Stanfield, Luca McDermott, Andrew V. Kelleghan,  
Benjamin J. Schwartz \* and Neil K. Garg \*

Polycyclic aromatic hydrocarbons (PAHs) are important compounds in materials chemistry, particularly for optoelectronic applications. One strategy for tuning PAH properties involves the net exchange of carbon atoms for heteroatoms, such as nitrogen. We report a comparative study of the well-known fluorophore 9,10-diphenylanthracene with an aza analog. The latter compound is accessed using a short sequence involving the use of two strained cyclic alkynes, benzyne and a 3,4-piperidine, in Diels–Alder cycloaddition sequences. Comparative studies of 9,10-diphenylanthracene and the aza-analog show how the addition of a single nitrogen atom impacts electrochemical and optical properties. Organic light-emitting diode (OLED) devices were prepared using both compounds, which showed that nitrogen substitution leads to an unexpected red shift in electroluminescence, likely due to exciplex formation between the active layer and the 4,4'-N,N'-bis[N-(1-naphthyl)-N-phenylamino]biphenyl (NPB) hole-transport layer. These studies highlight a unique approach to accessing heteroatom-containing PAHs, while underscoring the impact of heteroatoms on OLED device performance.

Received 5th June 2023,  
Accepted 12th July 2023

DOI: 10.1039/d3ma00280b

[rsc.li/materials-advances](https://rsc.li/materials-advances)

## Introduction

Polycyclic aromatic hydrocarbons (PAHs) have played an important role in the field of materials chemistry due to their valuable electronic properties and tunability.<sup>1–4</sup> Such tunability can be achieved either through modification of the periphery of the PAH to generate functionalized PAH derivatives or, alternatively, through modification of the PAH scaffold itself *via* the net exchange of carbon atoms for heteroatoms.<sup>5</sup> The latter strategy gives rise to polycyclic heteroaromatic molecules (PHAs), wherein at least one atom in the aromatic system is a heteroatom. The introduction of a heteroatom can have a significant effect on the electronic and physical properties of the material, allowing for tuning of material properties to suit a given application.<sup>6</sup> For example, the HOMO and LUMO of a material can be lowered by introduction of a heteroatom, and the HOMO/LUMO gap also can be altered.<sup>2,6</sup> In addition, when the heteroatom exhibits Lewis and/or Brønsted basicity, as with nitrogen, materials can become responsive to external stimuli, giving rise to valuable new properties.<sup>7</sup> Accordingly, new methodologies for the synthesis of

PAHs with nitrogen atom incorporation, as well as the study of these materials and their potential applications are highly desirable.

One PAH that has received a significant amount of attention for optoelectronic applications is 9,10-diphenylanthracene (DPA) (**1**, Fig. 1). Over the past century, **1** has been used as a sensitizer for chemiluminescence, such as glow sticks, as well as in OLEDs. A nitrogen atom-containing variant, aza-DPA **2**, was first synthesized in 1986<sup>8</sup> and has subsequently been prepared two more times in 1996<sup>9</sup> and 2012.<sup>10</sup> Although carbocycle **1** has been studied extensively, the photophysical and electronic properties of aza-DPA **2** have not been reported in the literature. We recognized that the chemistry of strained intermediates bearing cyclic alkynes,<sup>11,12</sup> such as those shown in Fig. 1b, could provide a new entryway to **2**. Heterocyclic alkynes and arynes, in particular, have been understudied in materials chemistry, despite being known for more than fifty years.<sup>8</sup>

Herein, we demonstrate a simple procedure for the synthesis of aza-DPA **2** that leverages a strain-promoted Diels–Alder cycloaddition of a strained azacyclic alkyne (Fig. 1c). Following development of this route, the electrochemical and optical properties of aza-DPA **2** were examined in comparison to **1**. Lastly, we prepared three-layer OLEDs consisting of an electron-blocking layer, an active layer comprised of either **1** or **2**, and a hole-blocking layer. Both photoluminescence and electroluminescence were compared to assess the impact of introducing a single nitrogen into the anthracene core on optoelectronic performance.

Department of Chemistry and Biochemistry, University of California at Los Angeles, Los Angeles, California 90095, USA. E-mail: [schwartz@chem.ucla.edu](mailto:schwartz@chem.ucla.edu), [neilgarg@chem.ucla.edu](mailto:neilgarg@chem.ucla.edu)

† Electronic supplementary information (ESI) available. See DOI: <https://doi.org/10.1039/d3ma00280b>



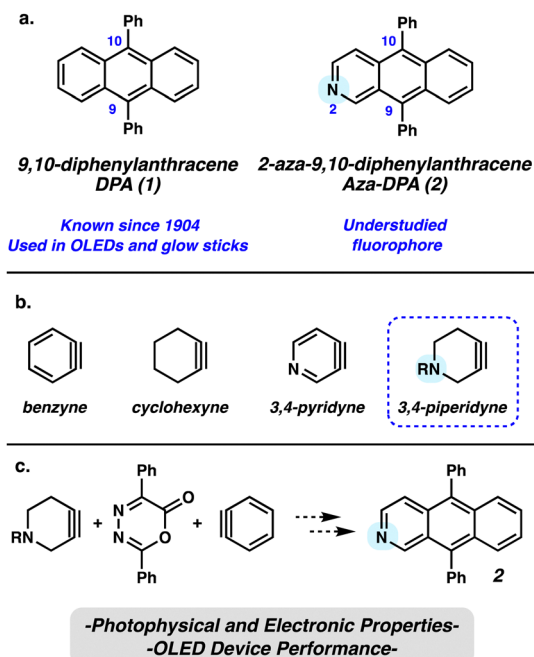


**Fig. 1** (a) Structures of PAHs **1** and **2**. (b) Strained cyclic alkyne intermediates, including benzyne and a 3,4-piperidyne. (c) Overview of current study, including reaction sequence involving strained intermediates to access **2** and studies of properties and device performance.

## Results and discussion

To initiate this study, we sought to prepare aza-DPA **2** by leveraging *in situ* generated strained cyclic alkynes. Our laboratory has previously developed a methodology that relies on controlled, sequential cycloadditions and retro-cycloadditions of oxadiazine building blocks to prepare unsymmetrical PAH-type scaffolds; we also performed computational studies.<sup>13,14</sup> The strategy obviates the need to use more traditional approaches, including those that use harsh reaction conditions,<sup>2,3</sup> and is amenable to heteroatom incorporation. In our optimized synthetic procedure shown in Fig. 2, azacyclic alkyne precursor **3**<sup>15</sup> was treated with CsF in the presence of oxadiazine **4**.<sup>16</sup> Via an initial Diels–Alder reaction (DA1) and subsequent retro-Diels–Alder reaction (rDA1) with loss of N<sub>2</sub>, bicycle **6** is formed as an inconsequential mixture of constitutional isomers. The mixture was then subjected to benzyne precursor **7** and CsF, ultimately delivering the desired core **9**. Similar to the prior transformation, the conversion of **6** to **9** takes place through a Diels–Alder/retro-Diels–Alder sequence (*i.e.*, DA2 to rDA2), but with loss of CO<sub>2</sub>. Both Diels–Alder/retro-Diels–Alder sequences proceed at ambient temperature using mild fluoride-based conditions. The final elaboration of **9** to aza-PAH **2** involved cleavage of the Boc protecting group using TFA, followed by mild oxidation using MnO<sub>2</sub>.<sup>17</sup> Aza-PAH **2** was purified three times by sublimation under reduced pressure prior to being used in subsequent optical and electrochemical characterization studies, including OLED fabrication.

With access to **2**, we performed comparative cyclic voltammetry (CV) studies to gauge how the presence of the nitrogen atom in the scaffold of **1** impacted electrochemical properties.

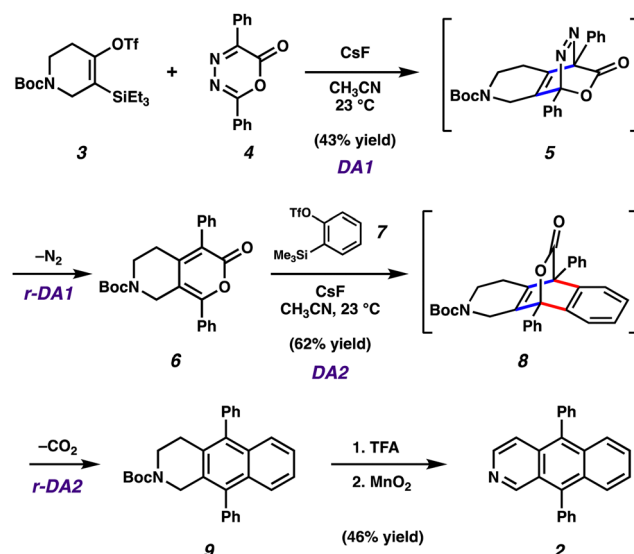


**Fig. 2** Synthesis of PHA **2** using Diels–Alder/Retro Diels–Alder (DA1/rDA1/DA2/rDA2) sequence.

As shown in Fig. 3, the reduction peak for both DPA **1** and aza-DPA **2** and were found to be reversible, with half wave potentials of  $-1.78$  V and  $-1.45$  vs. Ag/Ag<sup>+</sup>, respectively. Whereas DPA **1** had a reversible oxidation at peak potential of  $1.38$  V, the oxidation of aza-DPA **2** was found to be irreversible with a reductive peak potential of  $1.53$  V. These data suggest that replacement of a single C–H with a nitrogen atom leads to a material that is both easier to reduce and harder to oxidize. This change in atomic composition also leads to narrowing of the HOMO–LUMO energy gap,<sup>18</sup> which predicts a red-shift in the absorbance and emission energy of **2** relative to DPA **1**.

Absorption and photoluminescence (PL) spectra were collected for DPA **1** and aza-DPA **2** to assess the influence of the nitrogen substituent on optical properties (Fig. 4). Data were obtained using 10 mM solutions in toluene. Similar acene-like vibronic features were observed for **1** and **2** between 300–450 nm. However, aza-DPA **2** shows red-shifting in both the

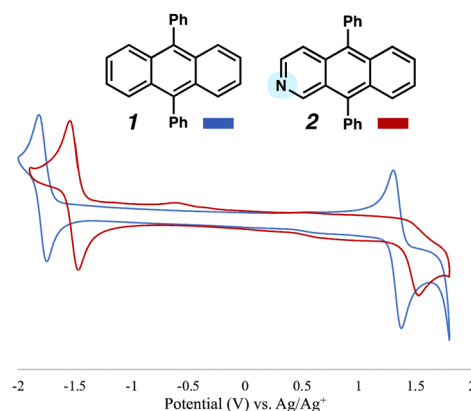


**Fig. 3** Comparative CV Data for DPA **1** (blue) and aza-DPA **2** (red). Introduction of the N heteroatom makes the system easier to reduce and harder to oxidize, as well as narrows the HOMO–LUMO gap.



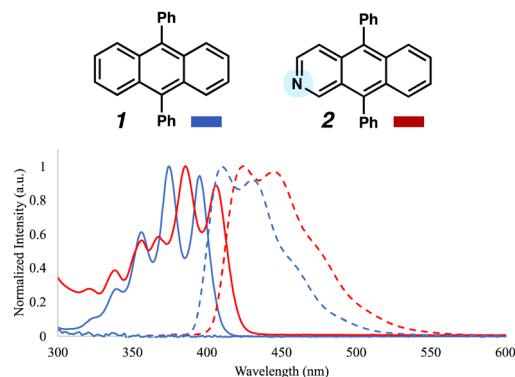


Fig. 4 Absorption (solid blue) and PL (dashed blue) spectra for DPA **1**. Absorption (solid red) and emission (dashed red) spectra for aza-DPA **2**. Both spectra were taken with the compounds dissolved in solution. As expected from the CV data in Fig. 3, the absorption and emission of **2** are redshifted from those of **1**.

absorption and emission spectra, which is consistent with the aforementioned narrowing of the HOMO–LUMO energy gap seen *via* CV.

To evaluate the influence of the nitrogen substituent on electroluminescent properties, OLEDs were fabricated using both DPA **1** and aza-DPA **2** as the active layers. These devices were comprised of three organic layers deposited sequentially *via* physical vapor deposition (PVD) without breaking vacuum (Fig. 5a), following a similar design to what has been used elsewhere to study this family of molecules.<sup>19–22</sup> The first organic layer, 4,4'-N,N'-bis[N-(1-naphthyl)-N-phenylamino]biphenyl (NPB) (30 nm), was deposited directly onto an indium tin oxide (ITO, anode) substrate as a hole transport layer (HTL). NPB is commonly used in commercial OLED applications due to its excellent hole transport properties as its relatively high-lying HOMO level (−5.5 eV) minimizes the hole injection barrier from the ITO anode (−4.7 eV).<sup>19</sup> At the same time, the high-lying LUMO level of NPB (−2.4 eV) efficiently blocks the transport of electrons that originate from the cathode end of the device. The second layer was comprised of the emissive/active layer, DPA **1** or aza-DPA **2**

(50 nm), where radiative electron-hole recombination is directed to take place. The third layer, 2,2',2''-(1,3,5-benzinetriyl)-tris(1-phenyl-1*H*-benzamidazole) (TPBi, 30 nm) has a relatively deep-lying HOMO level (−6.2 eV), which serves to efficiently block the transport of holes past the emissive layer. At the same time, the LUMO level for TPBi (−2.7 eV)<sup>20</sup> is located in the same energetic vicinity as the LiF/Al cathode (−2.9–3.5 eV),<sup>19</sup> which minimizes the barrier for electron injection from the device cathode into this layer. A thin (1 nm) layer of LiF was used as a dielectric screening layer, which has been shown to greatly enhance electron injection from the device cathode into such electron transport layers (ETLs).<sup>23</sup> Fig. 5a details the layered structure for the devices with the thicknesses of each layer. Energy level diagrams for the devices are shown for DPA **1** (Fig. 5b) and aza-DPA **2** (Fig. 5c) as the active layers.

Fig. 6a and b show electroluminescence (EL) spectra (turquoise curves) for devices based on these two active layers under modest driving voltages (**1**, 4 V and **2**, 7 V). This electroluminescence is compared to the PL spectra (dark blue curves) acquired by directly photoexciting the active layer in the devices. For the **1**-based devices shown in Fig. 6a, the same emission feature near 435 nm appears following both electrical and optical excitation in these devices. This peak emission wavelength corresponds to an energy gap of 2.85 eV, which matches remarkably well with the CV-derived HOMO–LUMO gap of 2.87 eV for **1**. Fig. 6b shows that the principal PL emission feature for the **2**-based devices is centered near 444 nm, which corresponds to a HOMO–LUMO gap of 2.79 eV for this molecule, which compares well to the CV-derived gap of 2.74 eV. In contrast to PL, the corresponding device EL spectrum with **2** as the active layer shows the 2.79 eV HOMO–LUMO emission as only a small shoulder, with a much larger emission feature centered at a lower energy near 2.42 eV (512 nm). This indicates that devices based on this compound are prone to emitting from a mid-gap state.

One plausible explanation for this red-shifted emission is that it corresponds to interface recombination between **2** and one of the small molecules located in an adjacent layer, forming an excited-state complex or exciplex. Exciplex emission is well-

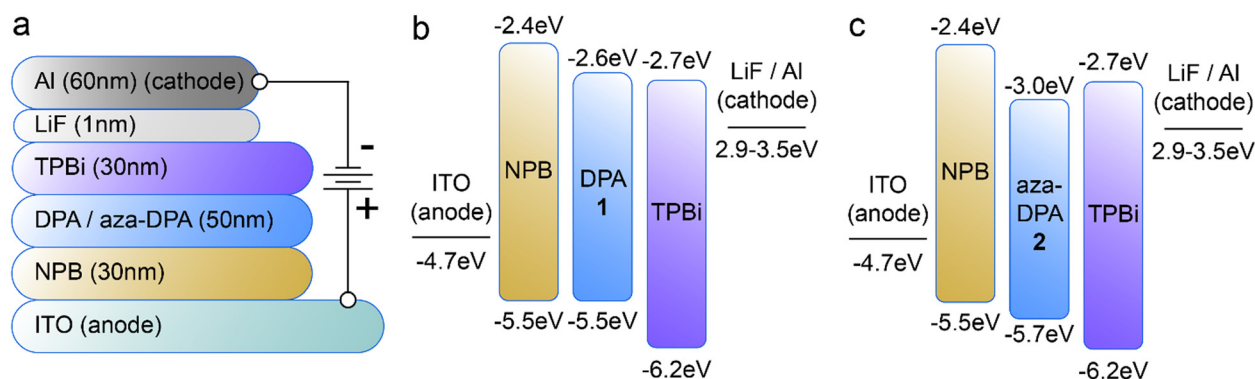
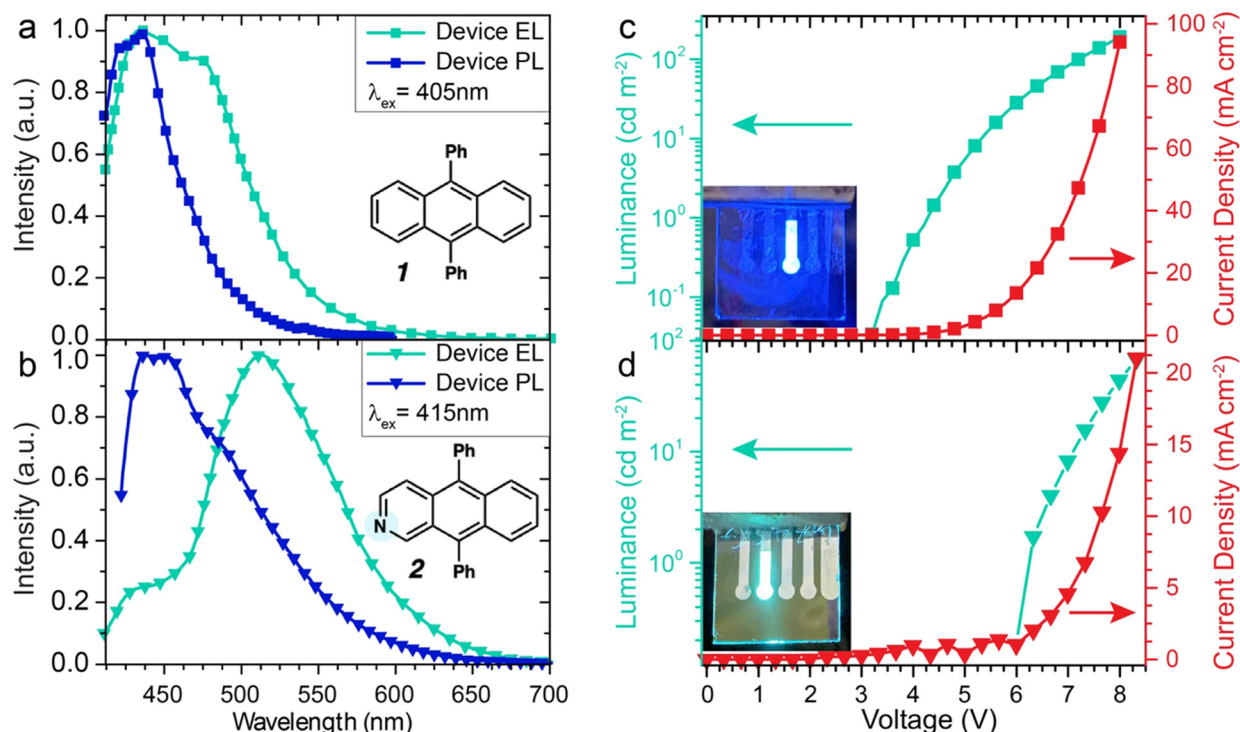


Fig. 5 (a) Schematic showing the layered structure of the OLED devices with their various layer thicknesses. NPB serves as an electron-blocking hole transport layer (HTL), while radiative electron-hole recombination occurs inside the (aza-)DPA emissive layer. TPBi serves as both a hole-blocking and electron transport layer (ETL). A thin, 1 nm layer of LiF is deposited below the aluminum electrode to enhance electron injection into the ETL. (b) Energy-level diagrams for the various OLED layers using DPA **1** as the active material. (c) Energy-level diagrams for the OLED layers using aza-DPA **2** as the active material.



**Fig. 6** (a) Electroluminescence (EL) and photoluminescence (PL) spectra of OLED devices (cf. Fig. 5 for structure) fabricated using **1** as the active layer. In contrast to Fig. 4, here the PL of the active emissive layer was directly measured by photoexciting inactive device samples at 405 nm, where the absorbance of **1** is strong. (b) EL and PL spectra for similar OLED devices fabricated using **2** as the active layer. PL of the emissive layer was selectively measured by photoexciting at 415 nm, where absorbance of the aza-DPA compound predominates. (c) Current density-voltage-luminance traces for OLED devices based on **1** as the emissive layer and (d) **2** as the emissive layer. Inset images show the electroluminescence from functioning devices.

studied in the organic light-emitting diode literature as a way of tuning the emission properties of an active layer.<sup>24,25</sup> It also has been recently shown that exciplex emission can be used to push beyond the theoretical external quantum efficiency (EQE) limit based on the spin-statistics involved with singlet emission in conventional fluorescent OLEDs.<sup>26,27</sup> In the current study, an exciplex consisting of a transition from the **2** LUMO energy of  $-2.96$  eV to the NPB HOMO at  $-5.5$  eV would be expected to luminesce with an energy of  $\sim 2.54$  eV, which is reasonably close to the observed EL emission of  $2.42$  eV (512 nm).

It is interesting to consider why exciplex emission is not present in the corresponding PL emission for **2**-based devices. The excitation wavelength of 415 nm was specifically chosen to maximize excitation of **2** while minimizing excitation in the neighbouring HLT/ELT layers. With excitation directed to occur in the emissive layer, the corresponding PL emission is primarily due to radiative recombination of **2** alone. In contrast to PL, during normal device operation, a driving voltage causes charge carriers to drift from each electrode towards the emissive layer. Fig. 5c shows there is a  $\sim 200$  meV energy barrier for hole injection from NPB into the **2** based emissive layer and this should lead to an accumulation of holes at the NPB/**2** interface in the form of NPB<sup>+</sup>. When the corresponding electrons reach the NPB/**2** interface as [aza-DPA]<sup>-</sup>, radiative recombination occurs specifically *via* relaxation of an excited state complex formed between the two species, which corresponds to a longer wavelength compared to **2**-based emission.

Fig. 6c and d show characteristic current density-voltage-luminance ( $J$ - $V$ - $L$ ) curves for the two sets of devices, with the luminance and current density plotted as a function of driving voltage. For the **1**-based devices, both the luminance and current density output for the DPA-based devices are higher, with a turn-on voltage around 3.4 V. In contrast, the **2**-based devices show a turn-on voltage of 6.0 V, which can be understood by considering the 200 meV energy barrier for hole injection from the NPB layer and the possible preference for exciplex emission with this molecule. Differences in the EL characteristics of these molecules demonstrate how simple atomic substitutions can dramatically change the propensity for exciplex formation.

## Conclusions

The incorporation of heteroatoms into PAH scaffolds provides an opportunity to tune electrochemical properties, optical properties, as well as device performance. We have demonstrated this in the context of the well-known fluorophore 9,10-diphenylanthracene (DPA, **1**) by preparing and studying aza-analog **2**. Aza-DPA **2** was synthesized using a facile cycloaddition cascade that hinges on the coupling of three fragments: a highly reactive azacyclic alkyne, a diphenyl oxadiazinone, and benzyne. Comparative studies of **1** and **2** show that introduction of a nitrogen atom into the DPA scaffold increases the oxidation potential and decreases the reduction potential and





the HOMO/LUMO gap. A red-shift is observed for both the absorption and emission spectra of **2** relative to **1**, which is consistent with the lowering of the HOMO/LUMO gap. Finally, OLED devices were prepared from both DPA **1** and aza-DPA **2**. Unlike compound **1**, the aza-substituted compound showed a shifted electroluminescence spectrum indicative of the formation of an exciplex species. These studies highlight a unique approach to accessing heteroatom-containing PAHs, while underscoring the impact of heteroatoms on OLED device performance.

## Data availability

Full details on the synthesis and characterization of compound **2** are accessible in the ESI†

## Author contributions

E. R. D., D. A. S., L. M., and A. V. K. designed and performed experiments and analyses. All authors participated in preparing the manuscript and discussions. B. J. S. and N. K. G. directed the investigations.

## Conflicts of interest

There are no conflicts to declare.

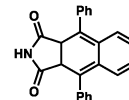
## Acknowledgements

The authors are grateful to the NIH-NIGMS (R01 GM123299 and R35 GM139593 for N. K. G.), the Trueblood Family (for N. K. G.), the NSF (DMR-2105896 for B. J. S. and DGE-2034835 for A. V. K.), and the Foote family (for A. V. K.). We thank Dr Melissa Ramirez (California Institute of Technology) for fruitful discussions regarding theoretical calculations. These studies were supported by shared instrumentation grants from the NSF (CHE-1048804) and the NIH NCRR (S10RR025631).

## References

- 1 J. E. Anthony, *Angew. Chem., Int. Ed.*, 2008, **47**, 452–483.
- 2 M. Stępień, E. Gońka, M. Żyła and N. Sprutta, *Chem. Rev.*, 2017, **117**, 3479–3716.
- 3 R. Dorel and A. M. Echavarren, *Eur. J. Org. Chem.*, 2017, 14–24.
- 4 A. J. Heeger, S. Kivelson, J. R. Schrieffer and W.-P. Su, *Rev. Mod. Phys.*, 1988, **60**, 781–850.
- 5 J. Wagner, P. Z. Crocomo, M. A. Kochman, A. Kubas, P. Data and M. Lindner, *Angew. Chem., Int. Ed.*, 2022, **61**, e202202232.

- 6 X.-Y. Wang, X. Yao, A. Narita and K. Müllen, *Acc. Chem. Res.*, 2019, **52**, 2491–2505.
- 7 V. M. Hertz, J. G. Massoth, M. Bolte, H.-W. Lerner and M. Wagner, *Chem. – Eur. J.*, 2016, **22**, 13181–13188.
- 8 F. Eiden and B. Wünsch, *Arch. Pharm.*, 1986, **319**, 886–889.
- 9 C. Bozzo and M. D. Pujol, *Heterocycl. Commun.*, 1996, **2**, 163–167.
- 10 S. J. Eum, Y. J. Cho, H. J. Kwon, B. O. Kim, S. M. Kim and S. M. Yoon, *U.S. Pat.* US8153279, 2012.
- 11 J. Shi, L. Li and Y. Li, *Chem. Rev.*, 2021, **121**, 3892–4044.
- 12 S. M. Anthony, L. G. Wonilowicz, M. S. McVeigh and N. K. Garg, *JACS Au*, 2021, **1**, 897–912.
- 13 E. R. Darzi, J. S. Barber and N. K. Garg, *Angew. Chem., Int. Ed.*, 2019, **58**, 9419–9424.
- 14 M. Ramirez, E. R. Darzi, J. S. Donaldson, K. N. Houk and N. K. Garg, *Angew. Chem., Int. Ed.*, 2021, **60**, 18201–18208.
- 15 The use of non-aromatic cyclic alkynes in the first cycloaddition allows for the controlled DA1/rDA1 to occur, thus delivering intermediate **6** and ultimately allowing for the assembly of unsymmetrical PAH scaffolds.
- 16 A. V. Kelleghan, K. A. Spence and N. K. Garg, *Org. Synth.*, 2020, **97**, 189–206.
- 17 A white crystalline side product was obtained and identified as the ring-contracted phthalimide shown below.



- 18 For relevant computational studies, see the ESI†.
- 19 J. Liu, H. Zhang, H. Dong, L. Meng, L. Jiang, L. Jiang, Y. Wang, J. Yu, Y. Sun, W. Hu and A. J. Heeger, *Nat. Commun.*, 2015, **6**, 10032.
- 20 C.-L. Wu, C.-H. Chang, Y.-T. Chang, C.-T. Chen, C.-T. Chen and C.-J. Su, *J. Mater. Chem. C*, 2014, **2**, 7188–7200.
- 21 W. J. Jo, K.-H. Kim, H. C. No, D.-Y. Shin, S.-J. Oh, J.-H. Son, Y.-H. Kim, Y.-K. Cho, Q.-H. Zhao, K.-H. Lee, H.-Y. Oh and S.-K. Kwon, *Synth. Met.*, 2009, **159**, 1359–1364.
- 22 H. Chen, W. Liang, Y. Chen, G. Tian, Q. Dong, J. Huang and J. Su, *RSC Adv.*, 2015, **5**, 70211–70219.
- 23 L. S. Hung, C. W. Tang and M. G. Mason, *Appl. Phys. Lett.*, 1997, **70**, 152–154.
- 24 H.-B. Kim and J.-J. Kim, *J. Inf. Disp.*, 2019, **20**, 105–121.
- 25 C.-H. Chang, S.-W. Wu, C.-W. Huang, C.-T. Hsieh, S.-E. Lin, N.-P. Chen and H.-H. Chang, *Jpn. J. Appl. Phys.*, 2016, **55**, 03CD02.
- 26 K. Goushi, K. Yoshida, K. Sato and C. Adachi, *Nat. Photonics*, 2012, **6**, 253–258.
- 27 K. Goushi and C. Adachi, *Appl. Phys. Lett.*, 2012, **101**, 023306.

